Building Effects on the P-Alert-Based Real-Time Shaking Map Determination

by Kai-Shyr Wang, Wei-An Chao, Himanshu Mittal, and Yih-Min Wu

ABSTRACT

Recently, the *P*-wave-alert-device (*P*-alert) network, which is a dense array of microelectromechanical system (MEMS) accelerometers that was developed and installed by National Taiwan University for the purposes of earthquake early warnings, has recorded a large number of strong-motion records for moderate-to-large earthquakes throughout Taiwan. However, many of these stations are mounted on the vertical walls of buildings in ways such that further studies of the sensor-structure interactions on recorded acceleration data are required before the data is used in the production of high-quality shake maps. In this study, we collect the free-field accelerograms recorded by the Taiwan Strong-Motion Instrumentation Program (TSMIP) network that were operated by the Central Weather Bureau (CWB), where MEMS accelerometers were in the vicinity. Then, we compare the peak ground acceleration (PGA) ratio (*R*-value) between *P*-alert and TSMIP stations. Finally, we demonstrate how to use the *R*-value correction on the *P*-alert data, in order to rapidly produce high-resolution shake maps for relief work to be done soon after major earthquakes. At present, the shake maps produced by the *P*-alert network are posted automatically in real time on Facebook and are provided to the National Science and Technology Center for Disaster Reduction (NCDR) in order to allow for their relief work. These timely products provide improved information for disaster risk reduction, emergency preparedness, and emergency response.

INTRODUCTION

Being located on the junction of two active subduction systems (namely Ryukyu to the north and Manilla to the south), Taiwan is a seismically active region. Active orogeny in Taiwan can be attributed to the collision between the Eurasian plate (EP) and the Philippine Sea plate (PSP; Lin and Watts, 2002; Wu *et al.*, 2009). Thousands of $\mathbf{M} > 2$ or 3 magnitude earthquakes occur in Taiwan every year as a result of collisions between the PSP and EP. In the past, many significant and devastating earthquakes occurred; examples include: the 1999 Chi-Chi M_w 7.6 earthquake (Chang *et al.*, 2000, 2007), the 2003 Chengkung M_w 6.8 earthquake (Wu *et al.*, 2006), the 2010 Jiasian M_w 6.3 earthquake (Huang *et al.*, 2011), and the February 2016 Meinong M_w 6.4 earthquake (Wu *et al.*, 2016; Kanamori *et al.*, 2017). The most recent significant earthquake, an earthquake of M_w 6.4, occurred on 6 February 2018 in the Hualien area of Taiwan. Because of the high level of seismicity, it is necessary to produce high-resolution shake maps in near-real time for the purposes of disaster risk reduction and emergency response. In Taiwan, the rapid reporting system (RRS) is based on the Central Weather Bureau Seismic Network (CWBSN, Hsiao *et al.*, 2011), which consists of more than 110 digital telemetered strong-motion seismic stations (Fig. 1a). The RRS system is designed to generate shake maps within a few minutes of the occurrence of a major earthquake. However, the distribution of the real-time CWBSN network is relatively sparse, making it difficult to produce high-resolution shake maps. For enhancement of the efficiency and resolution of shaking-map generation, a denser network of strong-motion instruments is required.

Recently, an earthquake early warning research group at National Taiwan University (Fig. 1b; Wu *et al.*, 2013; Hsieh *et al.*, 2015; Wu, 2015) developed a dense seismic network based on microelectromechanical system (MEMS) accelerometers. This *P*-alert network is capable of producing more detailed shake maps in near-real time (Hsieh *et al.*, 2014) and provides detailed strong ground motion information for research purposes. In order to check the usefulness of this *P*-alert network, we checked the impulsive velocity pulse at the W21B station during the 2016 Meinong earthquake and compared it with that at the nearby Taiwan Strong-Motion Instrumentation Program (TSMIP) station. The amplitudes of velocity pulses at both stations (*P*-alert and TSMIP) are comparable (Fig. 2); this indicates that the large displacement and velocity amplitudes at *P*-alert stations are not particularly anomalous and can be regarded as approximate free-field values (Kanamori *et al.*, 2017).

The *P*-alert accelerometers are installed on the vertical walls of buildings at different elevations in different buildings. Most of the sensors are placed on the first or second floor. In general, the sensors mounted on the building record both seismic signals and structure response. Therefore, the peak ground acceleration (PGA) recorded by these sensors is affected by sensor-structure-interaction and needs to be characterized properly when producing high-quality shake maps. In the present work, we collect the accelerograms from nearby sources: *P*-alert stations and free-field TSMIP stations. Then, a systematic investigation of the PGA ratio between *P*-alert and CWB TSMIP stations (*R*-value) is performed. Next, we develop a scaling law between the two systems. We then assess the accuracy of the shake maps produced

 doi: 10.1785/0220170252

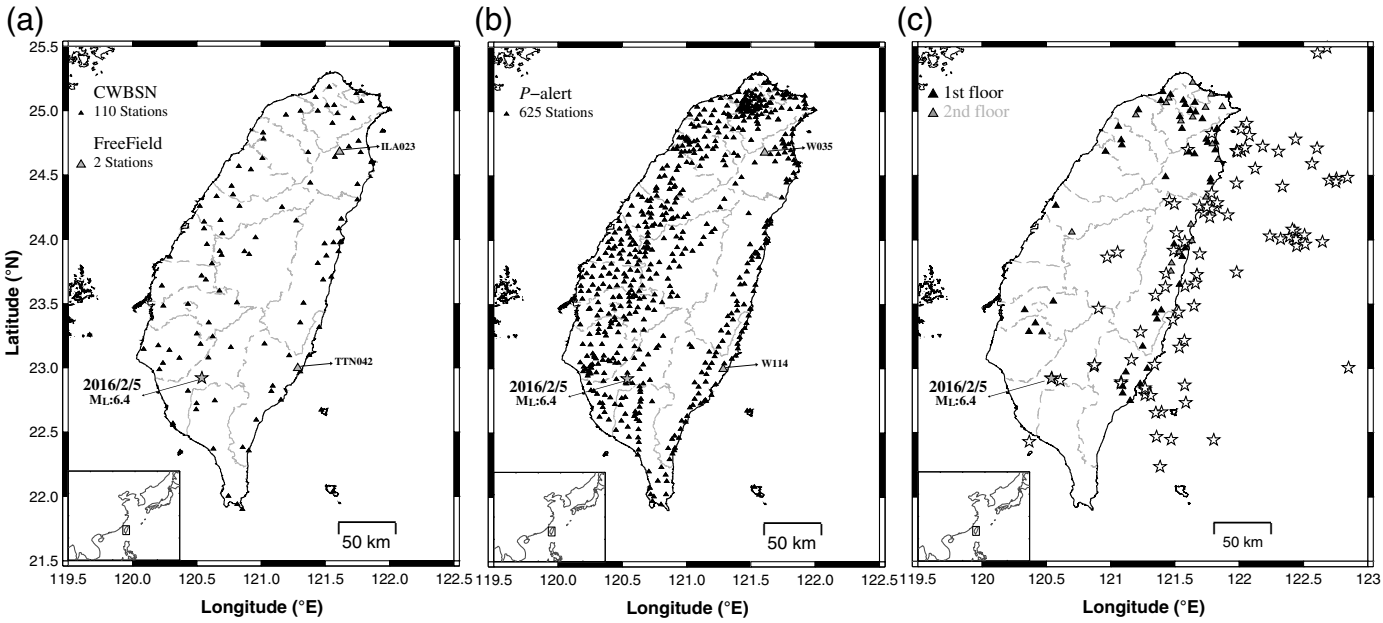

▲ **Figure 1.** Distributions of (a) Central Weather Bureau Seismic Network (CWBSN) and (b) *P*-alert seismic stations. (c) Triangles show the *P*-alert stations on first (black) and second (gray) floors nearly co-located with Taiwan Strong-Motion Instrumentation Program (TSMIP) seismic stations. Open stars represent the epicenters of 88 earthquake events used in this study. A large Asia map with marked studied area is shown in the inset. The location of the Meinong earthquake (M_w 6.4) is also shown.

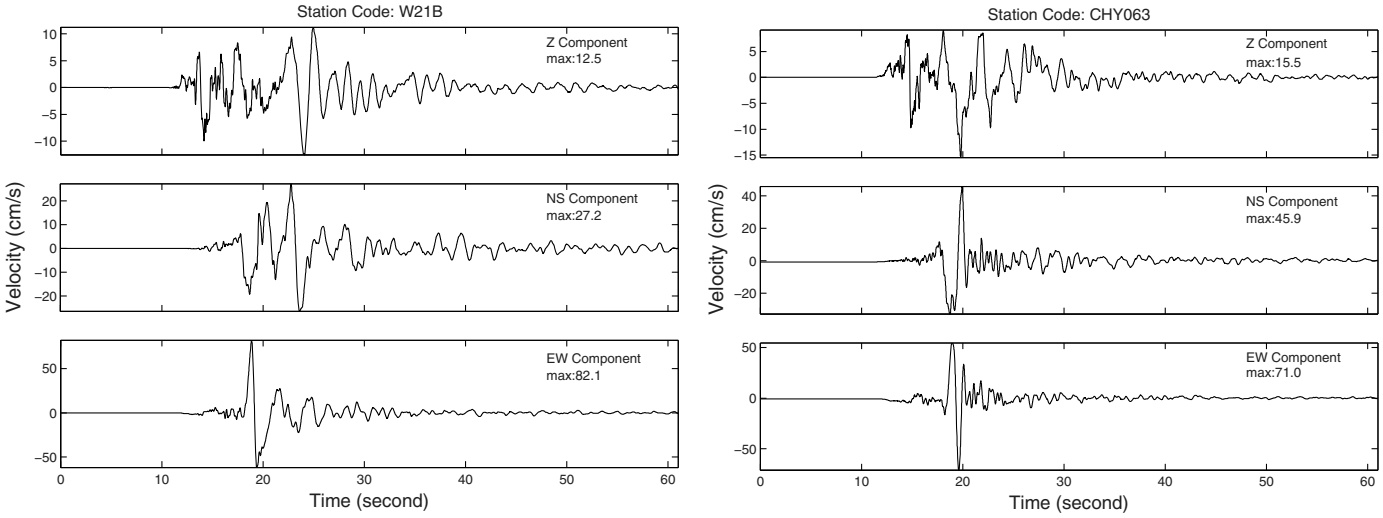

▲ **Figure 2.** Velocity pulse at W21B and nearby TSMIP station (CHY063) during the Meinong earthquake. The amplitude of velocity pulses at both stations (*P*-alert and TSMIP) is comparable, indicating that *P*-alert stations are not particularly anomalous and can be regarded as approximate free-field values.

by *P*-alert stations and finally discuss how the improved forecasts can be used for disaster risk reduction, emergency preparedness, and emergency response.

DATA PROCESSING AND RESULTS

The *P*-alert network currently consists of 625 low-cost MEMS accelerometers with a sampling rate of 100 Hz and a dense distribution throughout Taiwan, both in urban areas and along the active fault zones (Fig. 1b). For the purpose of examining the sensor-structure influence on the PGA estimation of the *P*-alert network, we collect strong-motion records from 88 earthquakes that were recorded by the TSMIP stations between August 2012 and December 2016. The magnitudes (M_L) of the collected events range from 5.0 to 6.7, and the chosen sites of the TSMIP stations are close to or nearly co-located (intersta-

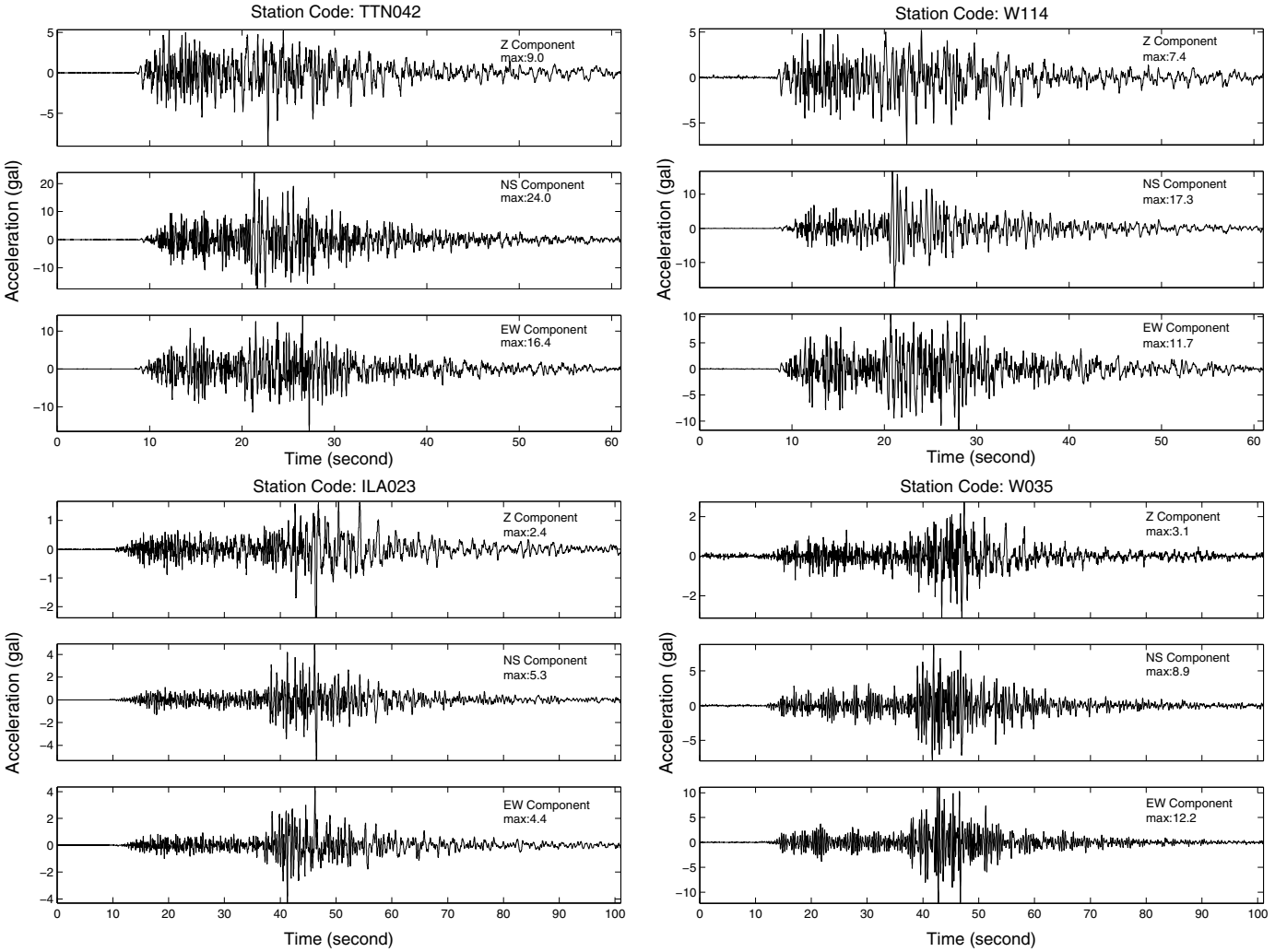

▲ **Figure 3.** Three-component strong-motion accelerograms from 5 February 2016 M_w 6.4 earthquake at the following station pairs: (a) TTN042–W114 and (b) ILA023–W035.

tion distance is less than 0.5 km) with the *P*-alert stations (Fig. 1c). Each TSMIP station is equipped with a force-balance accelerometer with a sampling rate of 200 Hz or higher. Both *P*-alert and TSMIP stations are designed with 16-bit resolution and a $\pm 2g$ full dynamic range. The three-component acceleration records are baseline corrected, and PGA values are measured from the maximum amplitudes on the unfiltered three-component accelerograms. As *P*-alert and TSMIP stations are roughly collocated, the PGA values are picked from the same seismic phases in both instrumentations. Secondly, most *P*-alert instruments have been placed on the first or second floors (Jan *et al.*, 2017) of two or three storied buildings (schools), so that there are less chances of PGA from different phases due to interference of surface waves and building response. These results can be inferred from Figure 3, where two station pairs are shown. For the TTN042/W114 station pair, PGA for the Z and north–south components occurs between 20 and 23 s, while for the east–west component, it is recorded around 27 s. A similar observation is found for the ILA023/W035 station pair. At each *P*-alert/TSMIP station pair, at least 12 PGA readings are applied for analysis of the PGA ratio (*R*-value) between *P*-alert and TSMIP stations.

The resultant *R*-values for the *P*-alert stations installed on first and second floors with mean values of 1.07 and 1.52 are shown in Figure 4 for each station that recorded at least 12 events. The highest and lowest anomalous *R*-values for the first floor are observed at stations W035 and W114, respectively (which may be due to improper installation of the *P*-alert device). Figure 3 shows examples of the original strong-motion accelerograms recorded by *P*-alert and TSMIP station pairs for the M_w 6.4 Meinong earthquake that occurred on 5 February 2016. For the W035–ILA023 station pair, the *R*-value reaches 2.8 in the east–west component. In contrast, for W114–TTN042, a minimal amplification of the acceleration seismogram was observed in the east–west component with an *R*-value of about 0.71 (Fig. 3). The difference between the *R*-value map for the *P*-alert corrected and TSMIP networks is shown in Figure 5. From Figure 5, an increase in *R*-values

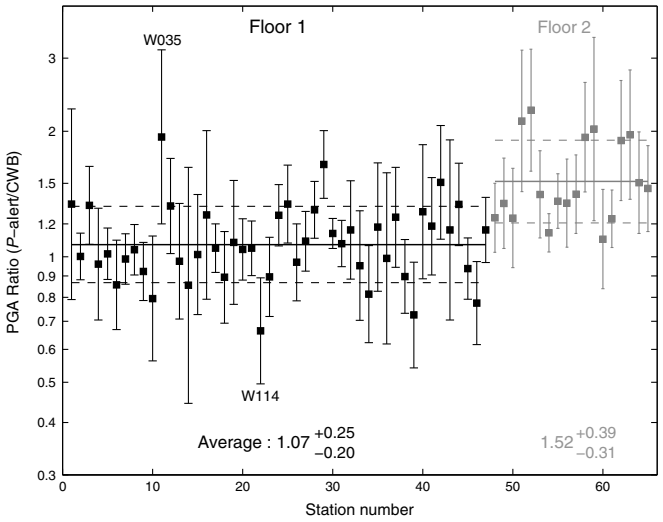

▲ **Figure 4.** The peak ground acceleration (PGA) ratio between *P*-alert and TSMIP stations (*R*-value) as a function of station number. Black and gray squares represent the data from first and second floors, respectively. The solid line shows the mean *R*-value, and the two dashed lines indicate the standard deviation.

is observed toward southern Taiwan, especially close to the epicenter of Meinong earthquake. In some areas, this difference exceeds 100 gal. In central Taiwan, the *R*-value difference is largely negative with respect to the CWBSN shake map. Leaving these two areas, the *R*-values for other regions in Taiwan are close, which means *R*-values are within ±50 gal. For two areas near the epicenter of Meinong earthquake, both increases and decreases may be attributed to the presence of basin or due to insufficient station coverage, as only 6–7 instruments are found in close vicinity. In general, differences in *R*-values might be attributed to sensor-structure-interaction effects, depending upon the location of the *P*-alert sensor in the building or improper installation of *P*-alert device in the building. The second reason for this difference may pertain to site effects (if stations are farther from each other), which will be different for each sensor depending upon specific site conditions. Though we have taken care in choosing *P*-alert and TSMIP stations, lower *R*-values are still obtained at some stations because site effects affect recordings drastically even at distances of a few hundred meters (Mittal, Kamal, *et al.*, 2013; Mittal, Kumar, and Kumar, 2013). However, further investigations will be needed to understand the differences. In general, the average *R*-values for the *P*-alert stations that were installed on first and second floors are 1.07 (+0.25, −0.20) and 1.52 (+0.39, −0.31), respectively.

DISCUSSION AND CONCLUSIONS

Response of a building to the earthquakes is highly dependent on shear-wave velocity and attenuation (Snieder and Safak, 2006). Response also relies heavily on building properties, as well as sub-surface coupling (Safak, 1995). Snieder and Safak (2006) used deconvolution of motion to remove the imprint of excitation and ground coupling and obtained consistent fundamental modes. They found that the response for the instruments placed on lower floors, such as the first or second floor, is quite consistent. Todorovska and Trifunac (2008) confirmed that monitoring only the changes in soil-structure frequency could skew the results regarding structural health monitoring (SHM). However, observing changes in fundamental fixed-base frequencies may provide robust results for SHM. The *R*-values for the devices on first and second floors determined by this study offer crucial information for eliminating sensor-structure interactions on *P*-alert acceleration data sets. After removing the sensor-structure-interaction effect, an approach has been adopted to include the CWBSN real-time stations located at free-field sites to provide the detailed shaking maps with better accuracy. Shake maps have proven to constitute a useful methodology to depict the shaking intensity in terms of PGA, peak ground velocity (PGV), and other spectral parameters. In some countries such as the U.S.A. and Taiwan, it is a routine practice to plot such shake maps after the occurrence of any moderate to severe earthquake (Wald, Quitoriano, Heaton, Kanamori, 1999; Wald, Quitoriano, Heaton, Kanamori, Scrivner, *et al.*, 1999; Lin and Wald, 2012; Wu *et al.*, 2016). García *et al.* (2012) presented a new version of shake map software that eliminates uncertainties by including the updated earthquake catalogs with information such as source finiteness, regional source locations, and ground-motion prediction equations (GMPE). Moratto *et al.* (2009) produced the real-time shake maps for Italy using different shaking parameters. Later on, Moratto and Saraò (2012) improved these real-time shake maps by including synthetic records. Legendre *et al.* (2017) plotted the shake maps for the Caucasas region using recorded waveforms from broadband seismic stations. They plotted shake maps in PGV only, as various uncertainties are introduced with the conversion of PGV to PGA. Allstadt *et al.* (2018) found that considering an approximate rupture extent instead of a point source in Shake Map generation, the landslide models were all successful at roughly identifying the area of highest hazard. Yang *et al.* (2018) used *P*-alert data for incorporation of a time-dependent anisotropic attenuation relationship with PGA, which can provide an accurate predicted PGA. This is a useful parameter to have before the arrival of the observed PGA that will give a consistent lead time for hazard assessment and emergency response and a predicted shake map that will converge faster to the final reported shake map. These kinds of studies are very important for a region like India, where instrumental recordings of ground motion are limited (Mittal, Kumar, and Kamal, 2013).

This study has also investigated the *R*-value for *P*-alert stations installed at ground level. Results show that the mean *R*-value is approximately equal to 1. Thus, *P*-alert data sets collected at ground level are also used in producing shake maps for later discussion. Figure 6 shows examples of the shake maps generated by the (a) *P*-alert system, (b) CWB system, (c) *P*-alert with corrected *R*-values, and (d) combination of corrected *P*-alert and CWB for the M_w 6.4 event that occurred on 5

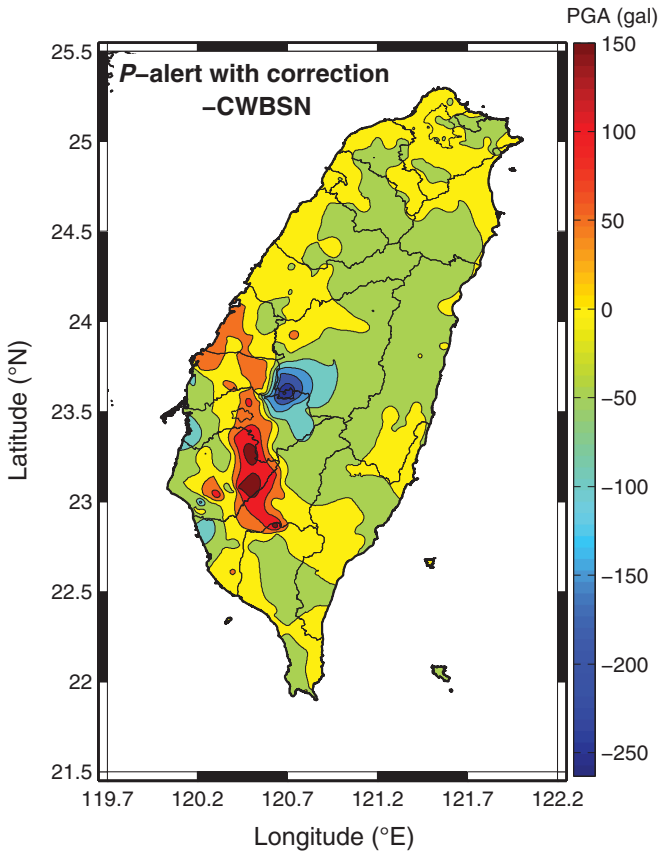

▲ **Figure 5.** The *R*-value map between *P*-alert corrected and TSMIP stations. An increase in *R*-values is observed toward southern Taiwan. In central Taiwan, the *R*-value difference is largely negative with respect to the CWBSN shake map. For all other regions, the *R*-values are within ±50 gal. This is the current *R*-value map for *P*-alert corrected and TSMIP stations.

February 2016. Obviously, the denser *P*-alert network produces a high-resolution shaking map compared to the map produced by the relatively sparse CWBSN network (Fig. 6a,b). In comparison between uncorrected (Fig. 6a) and corrected (Fig. 6c) *P*-alert shaking maps, there is only a small discrepancy that is attributed to structure response. Ideally, incorporating corrected *P*-alert acceleration data with the CWBSN network can provide the best resolutions of shaking maps, especially for local area and epicentral regions. For example, Figure 6d shows that results of PGAs are more high resolution in southwestern Taiwan.

In this study, for $M_L \geq 5.0$ events, average *R*-values for first and second floors are 1.07 and 1.52 (Fig. 4), respectively. When adding in the CWB system, we recommend that *P*-alert devices be installed either on the first floor or on the ground level. However, a few stations have relatively high or small *R*-values, which could be caused by equipment installation problems, anomalous building structure, or local site effects (where two types of instruments are away from each other). Future checks at station sites are needed to further understand the aforementioned problems. The *P*-alert stations with extreme *R*-values will be further investigated and reinstalled in the future.

P-alert devices can also be used for SHM, in comparison to traditional SHM accelerometers. Applications of *P*-alert devices to SHM have been studied by Yin *et al.* (2016) and Hsu *et al.* (2018). In their study, they used the Nakata *et al.* (2013) methodology to estimate the fundamental frequency of a steel building in a laboratory to monitor the health of the building. They compared the measured acceleration from a *P*-alert device to the acceleration measured by the low-frequency accelerometer calibration system (LFACS). They estimated the root mean square (rms) ratio by dividing the rms value from the *P*-alert device by that produced by the LFACS, and they found that rms ratios are close to 1.0 within the range between 0.8 and 10 Hz. After 15 Hz, rms ratios start to decrease, due to embedded low-pass filter of the *P*-alert device. Because the fundamental frequency of most buildings with 10 stories or less is greater than 1.0, these *P*-alert devices may be of good use in SHM applications.

Near-real-time shaking maps can promptly provide spatial distribution of PGA and seismic intensity following devastating earthquakes to conduct rapid hazard assessments. This study integrates both *P*-alert and CWB systems that can produce high-resolution shaking maps with better accuracy. However, currently correction of the sensor-structure-interaction effect only uses the mean *R*-values for the first and second floors. When the two types of instruments are collocated or very close to each other, the *R*-value is related to the stiffness, mass, and height of the building, as well as the installed station height. Snieder and Safak (2006) found similar results. If the relationships between the *R*-value and impact factors can be defined, the effects on each station can be corrected by using *R*-values to improve resolution. Furthermore, the *R*-values could be used to improve the accuracy of shake maps.

DATA AND RESOURCES

The strong-motion waveform records used in this study were obtained from the National Taiwan University (NTU) and Central Weather Bureau (CWB). The strong-motion records used in this study can be obtained upon request from CWB (http://www.cwb.gov.tw/eng/index.htm, last accessed August 2017). The *P*-alert waveform records are available to the public and can be downloaded from http://palert.earth.sinica.edu.tw/db/ (last accessed March 2018).

ACKNOWLEDGMENTS

This research has been supported by the Central Weather Bureau (CWB) and the Ministry of Science and Technology (MOST), Taiwan. This work was also financially supported by the NTU Research Center for Future Earth from The Featured Areas Research Center Program within the framework of the Higher Education Sprout Project by the Ministry of Education (MOE) in Taiwan. The constructive comments from two anonymous reviewers and Associate Editor Brendan Crowell helped to improve the article. The software package

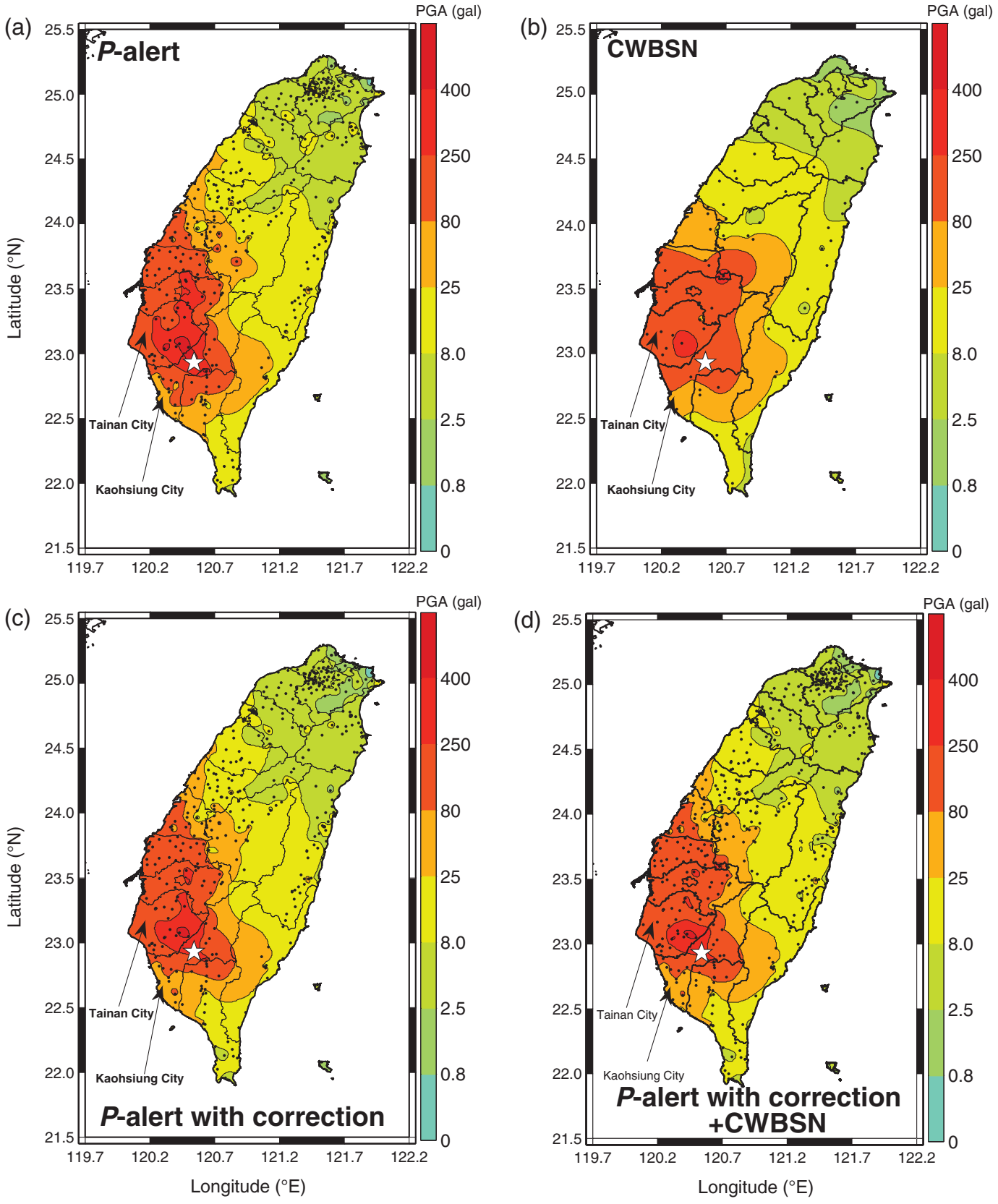

▲ **Figure 6.** Distributions of the PGA readings of the 5 February 2016 Meinong earthquake in southwestern Taiwan recorded from the (a) *P*-alert network, (b) CWBSN network, (c) *P*-alert network with correcting building effects, and (d) combination of corrected *P*-alert and CWBSN data.

Generic Mapping Tools (Wessel and Smith, 1998) was used in this study.

REFERENCES

Allstadt, K. E., R. W. Jibson, E. M. Thompson, C. I. Massey, D. J. Wald, J. W. Godt, and F. K. Rengers (2018). Improving near-real-time coseismic landslide models: Lessons learned from the 2016 Kaikōura, New Zealand, earthquake, *Bull. Seismol. Soc. Am.* **108,** 1649–1664, doi: 10.1785/0120170297.

Chang, C. H., Y. M. Wu, T. C. Shin, and C. Y. Wang (2000). Relocating the1999 Chi-Chi earthquake, Taiwan, *Terr. Atmos. Ocean. Sci.* **11,** 581–590.

Chang, C. H., Y. M. Wu, L. Zhao, and F. T. Wu (2007). Aftershocks of the 1999 Chi-Chi, Taiwan, earthquake: The first hour, *Bull. Seismol. Soc. Am.* **97,** 1245–1258, doi: 10.1785/0120060184.

García, D., R. T. Mah, K. L. Johnson, M. G. Hearne, K. D. Marano, K. W. Lin, D. J. Wald, C. B. Worden, and E. So (2012). ShakeMap Atlas 2.0: An improved suite of recent historical earthquake ShakeMaps for global hazard analyses and loss model calibration, in *World Conference on Earthquake Engineering* (https://www.iitk.ac.in/nicee/wcee/article/WCEE2012_2518.pdf, last accessed 2018/07/09).

Hsiao, N. C., Y. M. Wu, L. Zhao, D. Y. Chen, W. T. Huang, K. H. Kuo, T. C. Shin, and P. L. Leu (2011). A new prototype system for earthquake early warning in Taiwan, *Soil Dyn.. Earthq. Eng.* **31,** 201–208, doi: 10.1016/j.soildyn.2010.01.008.

Hsieh, C. Y., W. A. Chao, and Y. M. Wu (2015). An examination of the threshold-based earthquake early warning approach using a low-cost seismic network, *Seismol. Res. Lett.* **86,** 1664–1667, doi: 10.1785/0220150073.

Hsieh, C. Y., Y. M. Wu, T. L. Chin, K. H. Kuo, D. Y. Chen, K. S. Wang, Y. T. Chan, W. Y. Chang, W. S. Li, and S. H. Ker (2014). Low cost seismic network practical applications for producing quick shaking maps in Taiwan, *Terr. Atmos. Ocean. Sci.* **25,** 617–624, doi: 10.3319/TAO.2014.03.27.01(T).

Hsu, T. Y., R. C. Yin, and Y. M. Wu (2018). Evaluating post-earthquake building safety using economical MEMS seismometers, *Sensors* **18,** 1437, doi: 10.3390/s18051437.

Huang, H. H., Y. M. Wu, T. L. Lin, W. A. Chao, J. B. H. Shyu, C. H. Chan, and C. H. Chang (2011). The preliminary analysis of the 2010 M_w 6.3 Jiasian, Taiwan, earthquake sequence, *Terr. Atmos. Ocean. Sci.* **22,** 283–290.

Jan, J. C., W. A. Chao, Y. M. Wu, C. C. Chen, and C. H. Lin (2017). How well can we extract the permanent displacement from low-cost MEMS accelerometers?, *Sensors* **17,** 2643, doi: 10.3390/s17112643.

Kanamori, H., L. Ye, B. S. Huang, H. H. Huang, S. J. Lee, W. T. Liang, Y. Y. Lin, K. F. Ma, Y. M. Wu, and T. Y. Yeh (2017). A strong-motion hot spot of the 2016 Meinong, Taiwan, earthquake (M_w = 6.4), *Terr. Atmos. Ocean. Sci.* **28,** 637–650, doi: 10.3319/TAO.2016.10.07.01.

Legendre, C. P., T. L. Tseng, H. Mittal, C. H. Hsu, A. Karakhanyan, and B. S. Huang (2017). Complex wave propagation revealed by peak ground velocity maps in the Caucasus Area, *Seismol. Res. Lett.* **88,** 812–821, doi: 10.1785/0220160178.

Lin, K., and D. J. Wald (2012). Developing statistical fragility analysis framework for the USGS ShakeCast system for rapid post-earthquake assessment, *Proc. of the 15th World Conference on Earthquake Engineering (15WCEE)*, Lisbon, Portugal, 24–28 September.

Lin, A. T., and A. B. Watts (2002). Origin of the West Taiwan basin by orogenic loading and flexure of a rifted continental margin, *J. Geophys. Res.* **107,** 2185, doi: 10.1029/2001JB000669.

Mittal, H., A. Kumar, and Kamal (2013). Ground motion estimation in Delhi from postulated regional and local earthquakes, *J. Seismol.* **17,** no. 2, 593–605, doi: 10.1007/s10950-012-9340-5.

Mittal, H., A. Kumar, and A. Kumar (2013). Site effects estimation in Delhi from the Indian strong motion instrumentation network, *Seismol. Res. Lett.* **84,** 33–41.

Mittal, H., Kamal, A. Kumar, and S. K. Singh (2013). Estimation of site effects in Delhi using standard spectral ratio, *Soil Dyn.. Earthq. Eng.* **50,** 53–61, doi: 10.1016/j.soildyn.2013.03.004.

Moratto, L., and A. Saraò (2012). Improving ShakeMap performance by integrating real with synthetic data: Tests on the 2009 M_w = 6.3 L'Aquila earthquake (Italy), *J. Seismol.* **16,** 131–145.

Moratto, L., G. Costa, and P. Suhadolc (2009). Real-time generation of ShakeMaps in the southeastern Alps, *Bull. Seismol. Soc. Am.* **99,** 2489–2501.

Nakata, N., R. Snieder, S. Kuroda, S. Ito, T. Aizawa, and T. Kunimi (2013). Monitoring a building using deconvolution interferometry. I: Earthquake—Data analysis, *Bull. Seismol. Soc. Am.* **103,** 1662–1678, doi: 10.1785/0120120291.

Safak, E. (1995). Detection and identification of soil-structure interaction in buildings from vibration recordings, *J. Struct. Eng.* **121,** 899–906.

Snieder, R., and E. Safak (2006). Extracting the building response using interferometry: Theory and applications to the Millikan Library in Pasadena, California, *Bull. Seismol. Soc. Am.* **96,** 586–598.

Todorovska, M. I., and M. D. Trifunac (2008). Impulse response analysis of the Van Nuys 7-storey hotel during 11 earthquakes and earthquake damage detection, *Struct. Contr. Health Monit.* **15,** 90–116.

Wald, D. J., V. Quitoriano, T. H. Heaton, and H. Kanamori (1999). Relationships between peak ground acceleration, peak ground velocity and modified Mercalli intensity in California, *Earthq. Spectra* **15,** 557–564.

Wald, D. J., V. Quitoriano, T. H. Heaton, H. Kanamori, C. W. Scrivner, and C. B. Worden (1999). TriNet "ShakeMaps": Rapid generation of instrumental ground motion and intensity maps for earthquakes in southern California, *Earthq. Spectra* **15,** 537–556.

Wessel, P., and W. H. F. Smith (1998). New, improved version of Generic Mapping Tools released, *Eos Trans. AGU* **79,** 579.

Wu, Y. M. (2015). Progress on development of an earthquake early warning system using low-cost sensors, *Pure Appl. Geophys.* **172,** 2343–2351, doi: 10.1007/s00024-014-0933-5.

Wu, Y. M., D. Y. Chen, T. L. Lin, C. Y. Hsieh, T. L. Chin, W. Y. Chang, W. S. Li, and S. H. Ker (2013). A high-density seismic network for earthquake early warning in Taiwan based on low cost sensors, *Seismol. Res. Lett.* **84,** 1048–1054.

Wu, Y. M., Y. G. Chen, T. C. Shin, H. Kuochen, C. S. Hou, J. C. Hu, C. H. Chang, C. F. Wu, and T. L. Teng (2006). Coseismic vs. interseismic ground deformations, faults rupture inversion and segmentation revealed by 2003 M_w 6.8 Chengkung earthquake in eastern Taiwan, *Geophys. Res. Lett.* **33,** L02312, doi: 10.1029/2005GL024711.

Wu, Y. M., W. T. Liang, H. Mittal, W. A. Chao, C. H. Lin, B. S. Huang, and C. M. Lin (2016). Performance of a low-cost earthquake early warning system (P-Alert) during the 2016 M_L 6.4 Meinong (Taiwan) earthquake, *Seismol. Res. Lett.* **87,** 1050–1059, doi: 10.1785/0220160058.

Wu, Y. M., J. B. H. Shyu, C. H. Chang, L. Zhao, M. Nakamura, and S. K. Hsu (2009). Improved seismic tomography offshore northeastern Taiwan: Implications for subduction and collision processes between Taiwan and the southernmost Ryukyu, *Geophys. J. Int.* **178,** 1042–1054, doi: 10.1111/j.1365-246X.2009.04180.x.

Yang, B. M., T. C. Huang, and Y. M. Wu, (2018). ShakingAlarm: A Nontraditional regional earthquake early warning system based on time-dependent anisotropic peak ground-motion attenuation relationships, *Bull. Seismol. Soc. Am.* **108,** 1219–1230.

Yin, R. C., Y. M. Wu, and T. Y. Hsu (2016). Application of the low-cost MEMS-type seismometer for structural health monitoring: A pre-study, *Instrumentation and Measurement Technology Conference*

Proceedings (I2MTC), 2016 IEEE International, doi: 10.1109/I2MTC.2016.7520389.

Kai-Shyr Wang
Himanshu Mittal
Yih-Min Wu[1]
Department of Geosciences
National Taiwan University
No. 1, Roosevelt Road Sec.4
Taipei 10617, Taiwan
drymwu@ntu.edu.tw
yihmin.wu@gmail.com

Wei-An Chao
Department of Civil Engineering
National Chiao Tung University
No. 1001, University Road
Hsinchu 30010, Taiwan

Published Online 12 September 2018

[1] Also at Institute of Earth Sciences, Academia Sinica, No. 128 Academia Road, Section 2, Taipei 11529, Taiwan; also at NTU Research Center for Future Earth, National Taiwan University, Taipei 10617, Taiwan.